

CycleMLP: A MLP-like Architecture for Dense Prediction

Shoufa Chen¹ Enze Xie¹ Chongjian Ge¹ Ding Liang² Ping Luo¹
¹ The University of Hong Kong ² SenseTime Research

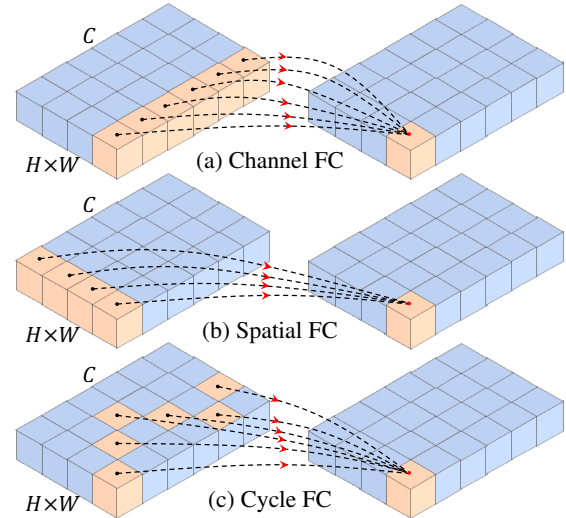
shoufach@connect.hku.hk pluo@cs.hku.hk

Abstract

This paper presents a simple MLP-like architecture, CycleMLP, which is a versatile backbone for visual recognition and dense predictions, unlike modern MLP architectures, e.g., MLP-Mixer [49], ResMLP [50], and gMLP [35], whose architectures are correlated to image size and thus are infeasible in object detection and segmentation. CycleMLP has two advantages compared to modern approaches. (1) It can cope with various image sizes. (2) It achieves linear computational complexity to image size by using local windows. In contrast, previous MLPs have quadratic computations because of their fully spatial connections. We build a family of models that surpass existing MLPs and achieve a comparable accuracy (83.2%) on ImageNet-1K classification compared to the state-of-the-art Transformer such as Swin Transformer [36] (83.3%), but using fewer parameters and FLOPs. We expand the MLP-like models’ applicability, making them a versatile backbone for dense prediction tasks. CycleMLP aims to provide a competitive baseline on object detection, instance segmentation, and semantic segmentation for MLP models. In particular, CycleMLP achieves 45.1 mIoU on ADE20K val, comparable to Swin (45.2 mIoU). Code is available at <https://github.com/ShoufaChen/CycleMLP>.

1. Introduction

Modeling in computer vision has been long dominated by convolutional neural networks (CNNs) [29, 43, 20] since the powerful hardware and highly optimized implementation of convolution were ready. However, inspired by successes in Natural Language Processing (NLP) field, Transformers [53] have been recently adopted into the computer vision community and made numerous breakthroughs [13, 51, 36]. Transformers [53] are built with multi-head self-attention layers, multi-layer perceptrons (MLPs), and skip connections [20]. More recently, building models solely on MLPs and skip connections without the self-attention layers has been a new trend for visual recognition tasks [49, 50, 35].



FC	$\mathcal{O}(HW)$	Scale Variable	ImgNet Top-1	COCO AP	ADE20K mIoU
Channel	HW	✓	79.4	35.0	36.3
Spatial	H^2W^2	✗	80.9	✗	✗
Cycle	HW	✓	81.6	41.7	42.4

Figure 1: **Motivation of Cycle Fully-Connected Layer (FC)** compared to Channel FC and Spatial FC. (a) Channel FC aggregates features in the channel dimension with spatial size ‘1’. It deals with various input scales but cannot learn spatial context. (b) Spatial FC [49, 50, 35] has a global receptive field in the spatial dimension. However, its parameter size is fixed and it has quadratic computational complexity to image scale. (c) Our proposed Cycle Fully-Connected Layer (Cycle FC) has linear complexity the same as channel FC and a larger receptive field than Channel FC.

The MLP-like models [49, 50, 35] are much simpler than Transformer-based models in: They replace the self-attention sub-layers by the purely fully-connected layers¹ (equal to the 1×1 convolution), removing the at-

¹MLP and FC are used interchangeably.

tention calculations. These models achieved surprisingly promising results on ImageNet [11] classification, which are even comparable to CNNs when trained on large scale datasets (*e.g.*, ImageNet-21K and JFT-300M).

Despite promising results on visual recognition tasks, these MLP-like models can not be used in other downstream tasks, *e.g.*, object detection and semantic segmentation due to the two challenges:

(1) Such models are composed of blocks with the same architectures, resulting in features with a single scale in low resolution. Thus, the non-hierarchical architectures make the model infeasible to provide pyramid feature representations.

(2) They can not deal with flexible input scales. They utilize the Spatial FC (Figure 1b), which is connected to all spatial points, for spatial information communication. Given a specific layer whose input is $x \in \mathbb{R}^{C_i \times H_i \times W_i}$ and output is $y \in \mathbb{R}^{C_o \times H_o \times W_o}$, where C, H, W denotes the channel, height and width, the weight² of spatial FC is $W_s \in \mathbb{R}^{H_i W_i \times H_o W_o}$. Thus, the structure of spatial FC is configured by $H \times W$, *i.e.*, the input spatial scale. Therefore, these models require a fixed input scale during both the training and validation stages. This requirement can be easily satisfied for ImageNet [11] classification because the input resolution of 224×224 is adopted for both training and evaluation as a popular setting [20, 43, 13, 36]. However, dense prediction tasks usually demand larger input resolution, *e.g.*, 512×512 for semantic segmentation on ADE20K [69]. Furthermore, some tasks adopt a multi-scale training strategy [5] and have different input resolutions between training and evaluation stages [34, 9]. In short, the applications of previous MLP models are limited due to that they can not deal with the inputs with flexible resolutions;

(3) The computational complexity of the Spatial FC is quadratic to image size, which makes it intractable for existing MLP-like models on high-resolution images.

To address the first challenge, we construct a hierarchical architecture to generate pyramid feature representations. For the second and third issues, we propose a novel variant of fully connected layer, named as *Cycle Fully-Connected Layer (Cycle FC)*, as illustrated in Figure 1c. The Cycle FC is capable of dealing with variable image scales and has linear computational complexity to image size.

Before the introduction of the Cycle FC, we first review channel FC layer (Figure 1a). The channel FC has already been widely adopted for channel information communication [32, 46, 20, 23]. Given the same input and output as Spatial FC, the weight of channel FC is $W_c \in \mathbb{R}^{C_i \times C_o}$, which is configured by two image-size agnostic parameters, C_i and C_o , making Channel FC able to deal with flexible image sizes. Moreover, it has a linear computational complexity to image size. However, the Channel FC is in-

²We omit *bias* here for discussion convenience.

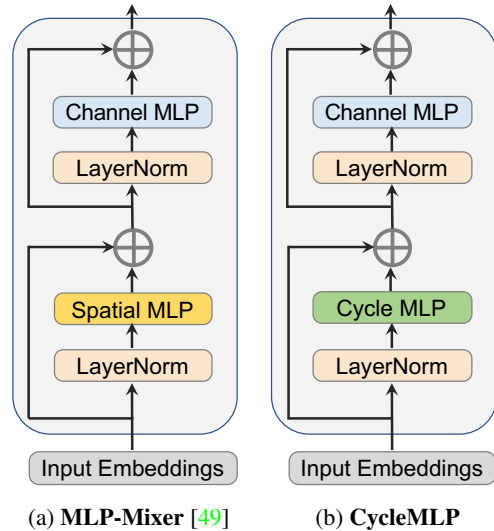


Figure 2: **Comparison of the MLP blocks.** MLP-Mixer (left) utilizes the vanilla MLP along spatial dimension for context aggregation. This operator cannot work when the input scale varies and has a quadratic computational complexity to image size. Our CycleMLP uses the *Cycle FC* for spatial projection which is capable of dealing with arbitrary scales and has a liner complexity.

feasible to aggregate context information due to its limited receptive field.

The motivation of Cycle FC is to enjoy channel FC’s merit of taking input with arbitrary resolution and linear computational complexity while enlarging its receptive field for context aggregation. To achieve this goal, our Cycle FC samples points in a cyclical style along the channel dimension (Figure 1c). In this way, Cycle FC has the same complexity (both the number of parameters and FLOPs) as channel FC, while increasing the receptive field simultaneously. We use Cycle FC to replace the Spatial FC for spatial context aggregation (*i.e.*, token mixing) and build a family of MLP-like models for both recognition and dense prediction tasks.

The contributions of this paper are as follows:

- We propose a new MLP-like operator, *Cycle Fully-Connected Layer (Cycle FC)*, which is a generic, plug-and-play replacement of Spatial FC, enabling MLP-like models to work in a scenario where input scales are flexible. Moreover, *Cycle FC* has a linear computational complexity to input resolution, while the complexity of Spatial FC is quadratic.
- With Cycle FC, we build a family of MLP-like architectures, learning pyramid feature representation for dense prediction tasks. To our knowledge, CycleMLP provides the first comprehensive baselines for both detection and segmentation tasks.

- We conduct extensive experiments on ImageNet classification, COCO object instance detection, and segmentation, and ADE20K semantic segmentation. The experimental results demonstrate that CycleMLP outperforms existing MLP-like models. Furthermore, CycleMLP is comparable to and sometimes better than CNNs and Transformers on dense predictions.

2. Related Work

CNN-based Models. Originally introduced over twenty years ago [30], convolutional neural networks (CNN) have been widely adopted since the success of the AlexNet [29] which outperformed prevailing approaches based on hand-crafted image features. There have been several attempts made to improve the design of CNN-based models. VGG [43] demonstrated a state-of-the-art performance on ImageNet via deploying small (3×3) convolution kernels to all layers. He *et al.* introduced skip-connections in ResNets [20], enabling a model variant with more than 1000 layers. DenseNet [24] connected each layer to every other layer in a feed-forward fashion, strengthening feature propagation and reducing the number of parameters. In parallel with these architecture design works, some other works also made significant contributions to the popularity of CNNs, including normalization [27, 2], data augmentation [10, 65, 66], etc.

Transformer-based Models. Transformers were first proposed by Vaswani *et al.* for machine translation and have since become the dominant choice in many NLP tasks [12, 54, 62, 4]. Recently, transformer have also led to a series of breakthroughs in computer vision community since the invention of ViT [13], and have been working as a *de facto* standard for various tasks, *e.g.*, image classification [13, 51, 64], detection and segmentation [56, 36, 67, 60], video recognition [57, 3, 1, 15] and so on. Moreover, there has also been lots of interest in adopting transformer to cross aggregate multiple modality information [39, 16, 14]. Furthermore, combining CNNs and transformers is also explored in [44, 31, 59, 52].

MLP-based Models. MLP-based models [49, 50, 35] differ from the above discussed CNN- and Transformer-based models because they resort to neither convolution nor self-attention layers. Instead, they use MLP layers over feature patches on spatial dimensions to aggregate the spatial context. These MLP-based models share similar macro structures but differ from each other in the detailed design of the micro block. In addition, MLP-based models provide more efficient computation than transformer-based models since they do not need to calculate affinity matrix using key-query multiplication. Concurrent to our work, S²-MLP [63] utilizes a spatial-shift operation for spatial information communication. The similar aspect between our work and S²-MLP lies in that we all conduct MLP operations along the

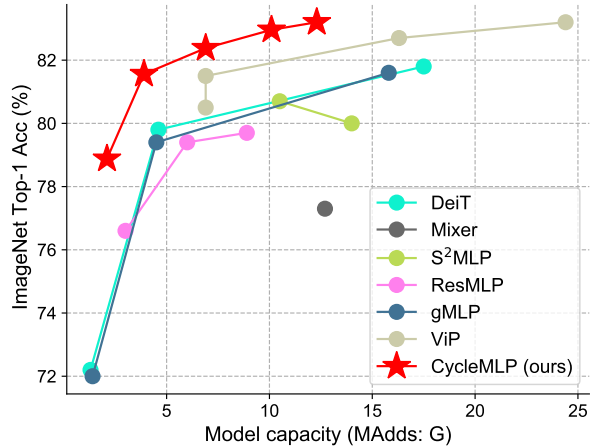


Figure 3: **ImageNet accuracy v.s. model capacity.** All models are trained on ImageNet-1K [11] without extra data. CycleMLP surpasses existing MLP-like models such as MLP-Mixer [49], ResMLP [50], gMLP [35], S²-MLP [63] and ViP [22].

channel dimension. However, our Cycle FC is different from S²-MLP in: (1) S²-MLP achieves communications between patches by splitting feature maps along channel dimension into several groups and shifting different groups in different directions. It introduces extra splitting and shifting operations on the feature map. On the contrary, we propose a novel operator-Cycle Fully-Connected Layer-for spatial context aggregation. It does not modify the feature map and is formulated as a generic, plug-and-play MLP unit that can be used as a direct replacement of vanilla without any adjustments. (2) We design a pyramid structure for and conduct extensive experiments on classification, object detection, instance segmentation, and semantic segmentation. However, the output feature map of S²-MLP has only one single scale in low resolution, which is unsuitable for dense prediction tasks. Only ImageNet classification is evaluated on S²-MLP. We will compare Cycle FC with S²-MLP in details in the Section 4.

3. Method

3.1. Overall Architecture

An overview of our proposed CycleMLP macro architecture is illustrated in Table 1. The design principle is mainly inspired by the philosophy of hierarchical Transformer [56, 36] models, which reduce the number of tokens at the transition layers as the network going deeper and increase the channel dimension. In this way, we can build a hierarchical architecture which is critical for dense prediction tasks [34, 69].

Given the raw input image with the size of $H \times W \times 3$,

our model first splits it into patches by a patch embedding module [13]. Each patch is then treated as a “token”. Specifically, we follow [15, 55] to adopt an overlapping patch embedding module with the window size 7 and stride 4. These raw patches are further projected to a higher dimension (denoted as C) by a linear embedding layer. Therefore, the overall patch embedding module generates the features with the shape of $\frac{H}{4} \times \frac{W}{4} \times C$.

Then, we sequentially apply several *Cycle FC* blocks, which is detailed in Section. 3.2, on the patch tokens. The blocks with the same architecture are stacked to form one *Stage* [20]. The number of tokens (feature scale) is maintained within each stage. At each stage *transition*, the channel capacity of the processed tokens is expanded while the number of tokens is reduced. This strategy effectively reduces the spatial resolution complexity. Overall, each of our model variants has four stages, and the output feature at the last stage has a shape of $\frac{H}{32} \times \frac{W}{32} \times C_4$. These stage settings are widely utilized in both CNN [43, 20] and Transformer [56, 36] models. Therefore, our proposed models can conveniently serve as a generic replacement for existing models.

3.2. Cycle FC Block

The Cycle FC block is illustrated in Figure 2b. Comparing with the pioneering MLP blocks [49] shown in Figure 2a, the key difference of Cycle FC block is that it utilize our proposed *Cycle Fully-Connected Layer (Cycle FC)* for spatial projection and advance the models in context aggregation and information communication. In detail, the Cycle FC block consists of three parallel Cycle FC operators, followed by a channel-MLP with two linear layers and a GELU [21] non-linearity in between. A Layer-Norm (LN) [2] layer is applied before both parallel Cycle FC layers and channel-MLP modules. A residual connection [20] is applied after each module. Formally, for a specific block ℓ , the tokens are processed as:

$$\hat{\mathbf{z}}^\ell = \text{Cycle FC}(\text{LN}(\mathbf{z}^{\ell-1})) + \mathbf{z}^{\ell-1}, \quad \ell = 1 \dots L \quad (1)$$

$$\mathbf{z}^\ell = \text{Channel-MLP}(\text{LN}(\hat{\mathbf{z}}^\ell)) + \hat{\mathbf{z}}^\ell, \quad \ell = 1 \dots L \quad (2)$$

where $\hat{\mathbf{z}}^\ell$ and \mathbf{z}^ℓ denote the output features of the Cycle FC-MLP module and the Channel-MLP module for block ℓ , respectively. LN denotes LayerNorm [2].

Our block design is purposely similar to ViT [13] except that we replace the multi-head self-attention (MSA) module in ViT [13] by our proposed Cycle FC operators for spatial context aggregation. Therefore, Cycle FC block can serve as a ready replacement for existing Transformer or MLP based architectures.

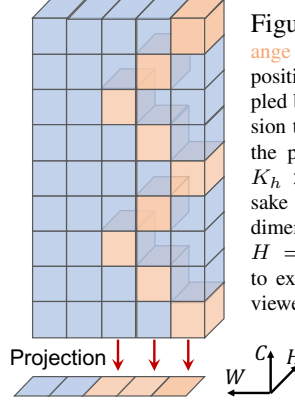


Figure 4: **Pseudo-Kernel:** Orange blocks denote the sampled positions. We project these sampled blocks along channel dimension to the spatial surface and get the pseudo kernel with the size $K_h \times K_w = 1 \times 3$. For the sake of simplicity, we omit batch dimension and take a feature with $H = 1$ for example. It is easy to extend to normal cases. Best viewed in color.

3.3. Cycle Fully-Connected Layer

Here we introduce the *Cycle Fully-Connected Layer (Cycle FC)* in details. The motivation behind Cycle FC is enabling MLP-like models to cope with variable input image scales, which is a common scenario in downstream dense prediction tasks. As illustrated in Figure 1 (a), the channel FC is configured by the *in* and *out* channel dimension at a specific layer. Its structure has nothing to do with the image scales. Hence, it is a scale-agnostic operation and can deal with variable input image scales, which is essential for dense prediction tasks. Moreover, another merit of channel FC is its linear computational complexity to the image scale. However, it has limited receptive fields that cannot aggregate enough context. As illustrated in the low part table of Figure 1, channel FC produces poor results due to the lack of context information.

To enlarge the receptive field while maintaining computation complexity, we propose a novel operator, named as Cycle Fully-Connected Layer (Cycle FC). As illustrated in Figure 1 (c), Cycle FC conducts the fully connection along channel dimension as channel FC does. However, unlike vanilla channel FC whose sampling points are located at the same spatial position for all channels, our Cycle FC samples points in a *stair-like* style.

Benefiting from this simple yet effective design, Cycle FC has the strictly equal complexity (in both FLOPs and the number of parameters) as vanilla channel FC. In addition, however, the receptive field is enlarged from a point to *pseudo-kernel*, which will be introduced in the following.

Pseudo-kernel. Here we introduce the concept of *pseudo-kernel*. As illustrated in Figure 4, we project the sampling points (orange blocks) of Cycle FC on the spatial surface and define the projection area as *pseudo-kernel* size.

Let $\mathbf{X} \in \mathbb{R}^{HW \times C_i}$ denote the input feature map, where HW represents its flattened height and width, and C_i denotes the input channels. For vanilla channel FC, the output feature $\mathbf{Y} \in \mathbb{R}^{HW \times C_o}$ can be obtained by:

	Output Size	Layer Name	CycleMLP				
			B1	B2	B3	B4	B5
Stage 1	$\frac{H}{4} \times \frac{W}{4}$	Overlapping	$S_1 = 4$				
		Patch Embedding	$C_1 = 64$				$C_1 = 96$
		CycleMLP Block	$E_1 = 4$ $L_1 = 2$	$E_1 = 4$ $L_1 = 2$	$E_1 = 8$ $L_1 = 3$	$E_1 = 8$ $L_1 = 3$	$E_1 = 4$ $L_1 = 3$
Stage 2	$\frac{H}{8} \times \frac{W}{8}$	Overlapping	$S_2 = 2$				
		Patch Embedding	$C_2 = 128$				$C_2 = 192$
		CycleMLP Block	$E_2 = 4$ $L_2 = 2$	$E_2 = 4$ $L_2 = 3$	$E_2 = 8$ $L_2 = 4$	$E_2 = 8$ $L_2 = 8$	$E_2 = 4$ $L_2 = 4$
Stage 3	$\frac{H}{16} \times \frac{W}{16}$	Overlapping	$S_3 = 2$				
		Patch Embedding	$C_3 = 320$				$C_3 = 384$
		CycleMLP Block	$E_3 = 4$ $L_3 = 4$	$E_3 = 4$ $L_3 = 10$	$E_3 = 4$ $L_3 = 18$	$E_3 = 4$ $L_3 = 27$	$E_3 = 4$ $L_3 = 24$
Stage 4	$\frac{H}{32} \times \frac{W}{32}$	Overlapping	$S_4 = 2$				
		Patch Embedding	$C_4 = 512$				$C_4 = 768$
		CycleMLP Block	$E_4 = 4$ $L_4 = 2$	$E_4 = 4$ $L_4 = 3$	$E_4 = 4$ $L_4 = 3$	$E_4 = 4$ $L_4 = 3$	$E_4 = 4$ $L_4 = 3$
Parameters (M)			15.2	26.8	38.4	51.8	75.7
FLOPs (G)			2.1	3.9	6.9	10.1	12.3

Table 1: **Instantiations of the CycleMLP with varying complexity.** The E_i and L_i denote the *expand ratio* and *number of repeated layers*. Our design principle is inspired by the philosophy of ResNet [20], where the channel dimension increases while the spatial resolution shrinks with the layer going deeper.

$$\mathbf{Y}_{i,j} = \sum_{c=0}^{C_i-1} \mathcal{F}_{j,c}^T \cdot X_{i,c} \quad , \quad (3)$$

where $\mathcal{F} \in \mathbb{R}^{C_i \times C_o}$ is the learnable weight of channel FC and is optimized through the backpropagation [42]. i and j are the spatial and channel index, respectively.

The core design of the Cycle FC is that we change the sampling index of \mathbf{X} along the channel dimension from the fixed point i to a pseudo-kernel window $i + c\%S_p$, which is centered at i and has a perceptive field of S_p . Hence, the operation of Cycle FC is defined as:

$$\mathbf{Y}_{i,j} = \sum_{c=0}^{C_i-1} \mathcal{F}_{j,c}^T \cdot X_{i+c\%S_p,c} \quad , \quad (4)$$

where $S_p = K_h \times K_w$ is the pseudo-kernel size.

3.4. Discussion

Cycle FC can perceive the neighboring context while maintaining the same complexity as channel FC, regarding both the number of parameters and FLOPs. Thus, Cycle FC is a generic and plug-and-play operator to facilitate spatial context aggregation. Note that when pseudo-kernel size is configured as 1×1 , Cycle FC degenerates into the vanilla channel FC.

3.5. Architecture Variants

We build a family of MLP-like models, CycleMLP, based on Cycle FC to cover a wide spectrum of model complexities (from 2.1G to 12.3G FLOPs). We configured the number of parallel Cycle FC branches as three, and the pseudo-kernel size as 1×3 , 3×1 , and 1×1 , which is inspired by the factorization of convolution [47] and criss-cross attention [26]. These models are scaled up from CycleMLP-B1 to CycleMLP-B5 by adapting three architecture-related hyper-parameters:

- S_i : the stride of the transition layer at Stage i ;
- C_i : the token channel dimension at Stage i ;
- L_i : the number of blocks at Stage i ;
- E_i : the expansion ratio at Stage i .

The details of the architecture hyper-parameters are shown in Table 1. All model instantiations share the same hierarchical macro structure, which consists of 4 stages, following the design principle of ResNets [20].

4. Experiments

In this section, we first examine CycleMLP by conducting experiments on ImageNet-1K [11] image classification. Then, we present a bunch of baseline models achieved by CycleMLP in dense prediction tasks, *i.e.*, COCO [34] object detection, instance segmentation, and ADE20K [69] semantic segmentation.

4.1. ImageNet-1K Classification

In this subsection, we present experimental results on image classification. We also conduct extensive ablation studies to understand the proposed CycleMLP.

Settings. We train our models on the ImageNet-1K dataset [11], which contains 1.2M training images and 50K validation images evenly spreading 1,000 categories. We follow the standard practice in the community by reporting the top-1 accuracy on the validation set. Our code is implemented based on PyTorch [38] framework and heavily relies on the timm [58] repository. For apple-to-apple comparison, our training strategy is mostly adopted from DeiT [51], which includes RandAugment [10], Mixup [66], Cutmix [65] random erasing [68] and stochastic depth [25]. The optimizer is AdamW [37] with the momentum of 0.9 and weight decay of 5×10^{-2} by default. The cosine learning rate schedule is adopted with the initial value of 1×10^{-3} . All models are trained for 300 epochs on 8 Tesla V100 GPUs with a total batch size of 1024.

Further kernel optimization for Cycle FC may bring a faster speed but is beyond the scope of this work.

Comparison with MLP-like Models. We first compare CycleMLP with existing MLP-like models and the results are summarized in Table 2 and Figure 3. The accuracy-FLOPs tradeoff of CycleMLP consistently outperforms existing MLP-like models [49, 50, 35, 18, 63, 22] under a wide range of FLOPs, which we attribute to the effectiveness of our Cycle FC. Specifically, compared with one of the pioneering MLP work, *i.e.*, gMLP [35], CycleMLP-B2 achieves the same top-1 accuracy (81.6%) as gMLP-B while reduces more than $3 \times$ FLOPs (3.9G for CycleMLP-B2 and 15.8G for gMLP-B). Furthermore, compared with existing SOTA MLP-like model, *i.e.*, ViP [22], our model CycleMLP-B5 utilizes only a half FLOPs (12.3G) as ViP-Large/7 (24.4G, the largest one of ViP family) while maintains the same top-1 accuracy (83.2%).

It is noted that all previous MLP-like models listed in Table 2 do not conduct experiments on dense prediction tasks due to the incapability of dealing with variable input scales, which is discussed in Sec 1. However, CycleMLP solved this issue by adopting Cycle FC. The experimental results on dense prediction tasks are presented in Sec 4.3 and Sec 4.4.

Comparison with SOTA Models. Table 3 further compares CycleMLP with previous state-of-the-art CNN, Transformer and Hybrid architectures. It is interesting to see that CycleMLP models achieve comparable performance to Swin Transformer [36], which is the state-of-the-art Transformer-based model. Specifically, CycleMLP-B5 achieves almost equal top-1 accuracy (83.2%) as Swin-B (83.3%) with slightly fewer parameters and FLOPs. The concurrent work GFNet [41] utilizes the fast Fourier transform (FFT) [8] to learn spatial information and achieves

Model	Date	Param	FLOPs	Top-1 (%)
EAMLP-14 [18]	arXiv:2105	30M	-	78.9
EAMLP-19 [18]		55M	-	79.4
Mixer-B/16 [49]	arXiv:2105	59M	12.7G	76.4
Mixer-B/16 [49] [†]		59M	12.7G	77.3
ResMLP-S12 [50]	arXiv:2105	15M	3.0G	76.6
ResMLP-S24 [50]		30M	6.0G	79.4
ResMLP-B24 [50]		116M	23.0G	81.0
gMLP-Ti [35]	arXiv:2105	6M	1.4G	72.3
gMLP-S [35]		20M	4.5G	79.6
gMLP-B [35]		73M	15.8G	81.6
S ² -MLP-wide [63]	arXiv:2106	71M	14.0G	80.0
S ² -MLP-deep [63]		51M	10.5G	80.7
ViP-Small/14 [22]	arXiv:2106	30M	6.9G	80.5
ViP-Small/7 [22]		25M	6.9G	81.5
ViP-Medium/7 [22]		55M	16.3G	82.7
ViP-Large/7 [22]		88M	24.4G	83.2
CycleMLP-B1	arXiv:2107	15M	2.1G	78.9
CycleMLP-B2		27M	3.9G	81.6
CycleMLP-B3		38M	6.9G	82.4
CycleMLP-B4		52M	10.1G	83.0
CycleMLP-B5		76M	12.3G	83.2

Table 2: **ImageNet-1K classification for MLP-like models.** The “Date” column shows the initial report release date. *E.g.*, “arXiv 2105” denotes “May, 2021”. [†] is implemented by [35]

similar performance as CycleMLP on ImageNet-1K classification. However, the architecture of GFNet is correlated with the input resolution, and extra operation (parameter interpolation) is required when input scale changes, which may hurt the performance of dense prediction. We will thoroughly compare CycleMLP with GFNet in Sec 4.4 on ADE20K.

4.2. Ablation Study

In this subsection, we conduct extensive ablation studies to analyze each component of our design. Unless otherwise stated, We adopt CycleMLP-B2 instantiation in this subsection.

Cycle Fully-Connected Layer To clearly demonstrate the advantage of the Cycle FC, we compare CycleMLP-B2 with two other baseline models equipped with channel FC and Spatial FC as spatial context aggregation operators, respectively. The details of these operators and the comparison results are presented in Figure 1. CycleMLP-B2 outperforms the counterparts built on both Spatial and Channel FC for ImageNet classification, COCO object detection, instance segmentation, and ADE20K semantic segmentation. The results validate that Cycle FC is capable of serving as a general-purpose, plug-and-play operator for spatial infor-

Model	Family	Scale	Param	FLOPs	Top-1 (%)
ResNet18 [20]	CNN	224 ²	12M	1.8G	69.8
EffNet-B3 [48]	CNN	300 ²	12M	1.8G	81.6
PVT-T [56]	Trans	224 ²	13M	1.9G	75.1
GFNet-H-Ti [41]	FFT	224 ²	15M	2.0G	80.1
CycleMLP-B1	MLP	224 ²	15M	2.1G	78.9
ResNet50 [20]	CNN	224 ²	26M	4.1G	78.5
RegNetY-4G [40]	CNN	224 ²	21M	4.0G	80.0
DeiT-S [51]	Trans	224 ²	22M	4.6G	79.8
BoT-S1-50 [44]	Hybrid	224 ²	21M	4.3G	79.1
PVT-S [56]	Trans	224 ²	25M	3.8G	79.8
Swin-T [36]	Trans	224 ²	29M	4.5G	81.3
GFNet-H-S [41]	FFT	224 ²	32M	4.5G	81.5
CycleMLP-B2	MLP	224 ²	27M	3.9G	81.6
ResNet101 [20]	CNN	224 ²	45M	7.9G	79.8
RegNetY-8G [40]	CNN	224 ²	39M	8.0G	81.7
BoT-S1-59 [44]	Hybrid	224 ²	34M	7.3G	81.7
PVT-M [56]	Trans	224 ²	44M	6.7G	81.2
CycleMLP-B3	MLP	224 ²	38M	6.9G	82.4
GFNet-H-B [41]	FFT	224 ²	54M	8.4G	82.9
Swin-S [36]	Trans	224 ²	50M	8.7G	83.0
PVT-L [56]	Trans	224 ²	61M	9.8G	81.7
CycleMLP-B4	MLP	224 ²	52M	10.1G	83.0
ViT-B/16 [13]	Trans	384 ²	86M	55.4G	77.9
DeiT-B [51]	Trans	224 ²	86M	17.5G	81.8
DeiT-B [51]	Trans	384 ²	86M	55.4G	83.1
Swin-B [36]	Trans	224 ²	88M	15.4G	83.3
CycleMLP-B5	MLP	224 ²	76M	12.3G	83.2

Table 3: **Comparison with SOTA models on ImageNet-1K without extra data.** Models with similar complexity are grouped together for comparison. The proposed CycleMLP consistently achieves comparable or even better performance to SOTA models with the matching computation and parameter constraint.

mation communication and context aggregation.

Table 4 further details the ablation study on the structure of CycleMLP block. It is observed that the top-1 accuracy drops significantly after removing one of the three parallel branches, especially when discarding the 1×3 or 3×1 branch. To eliminate the probability that the fewer parameters and FLOPs cause the performance drop, we further use two same branches (denoted as “ $\checkmark\checkmark$ ” in Table 4) and one 1×1 branch to align the parameters and FLOPs. The accuracy still drops relative to CycleMLP, which further demonstrates the necessity of these three unique branches.

Resolution adaptability. One remarkable advantage of CycleMLP lies in that they can take images at arbitrary resolutions as input without any modification. On the contrary, the contemporary work GFNet [41] needs to interpolate the learnable parameters on the fly when the input scale is different from the one for training. We compare

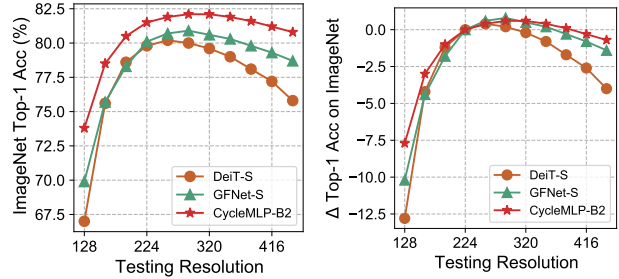


Figure 5: **Resolution adaptability.** All models are trained on 224×224 and evaluated on various resolutions without fine-tuning. **Left:** Absolute top-1 accuracy; **Right:** Accuracy difference relative to that tested on 224×224 . The superiority of CycleMLP’s robustness becomes more significant when scale varies to a greater extent.

the resolution adaptability by directly evaluating models at a broad spectrum of resolutions using the weight pre-trained on 224×224 , without fine-tuning. Figure 5 (left) shows that the absolute Top-1 accuracy on ImageNet and (right) shows the accuracy differences between one specific resolution and the resolution of 224×224 . Compared with DeiT and GFNet, CycleMLP is more robust when resolution varies. In particular, at the 128×128 , CycleMLP saves more than 2 points drop compared to GFNet. Furthermore, at higher resolution, the performance drop of CycleMLP is less than GFNet. Note that the superiority of CycleMLP becomes more significant when the resolution changes to a greater extent.

1×3	3×1	1×1	Params	FLOPs	Top-1 Acc
\checkmark		\checkmark			76.69
	\checkmark	\checkmark	24.5M	3.6G	76.94
\checkmark	\checkmark				78.00
$\checkmark\checkmark$		\checkmark	26.8M	3.9G	76.93
	$\checkmark\checkmark$	\checkmark			77.30
\checkmark	\checkmark	\checkmark	26.8M	3.9G	78.60

Table 4: **Ablation on three parallel branches.** We adopt CycleMLP-B2 variant for this ablation study, and models are trained for 100 epochs. Double check marks ($\checkmark\checkmark$) denotes two same branches.

4.3. Object Detection and Instance Segmentation

Settings. We conduct object detection and instance segmentation experiments on COCO [34] dataset, which contains 118K and 5K images for train and validation splits. We adopt the mmdetection [6] toolbox for all experiments in this subsection. To evaluate the our CycleMLP backbones, we adopt two widely used detectors, *i.e.*, RetinaNet [33] and Mask R-CNN [19]. All backbones

Backbone	RetinaNet 1×							Mask R-CNN 1×						
	Param	AP	AP ₅₀	AP ₇₅	AP _S	AP _M	AP _L	Param	AP ^b	AP ^b ₅₀	AP ^b ₇₅	AP ^m	AP ^m ₅₀	AP ^m ₇₅
ResNet18 [20]	21.3M	31.8	49.6	33.6	16.3	34.3	43.2	31.2M	34.0	54.0	36.7	31.2	51.0	32.7
PVT-Tiny [56]	23.0M	36.7	56.9	38.9	22.6	38.8	50.0	32.9M	36.7	59.2	39.3	35.1	56.7	37.3
CycleMLP-B1	24.9M	38.6	59.1	40.8	21.9	41.8	50.7	34.8M	39.4	61.4	43.0	36.8	58.6	39.1
ResNet50 [20]	37.7M	36.3	55.3	38.6	19.3	40.0	48.8	44.2M	38.0	58.6	41.4	34.4	55.1	36.7
PVT-Small [56]	34.2M	40.4	61.3	43.0	25.0	42.9	55.7	44.1M	40.4	62.9	43.8	37.8	60.1	40.3
CycleMLP-B2	36.5M	40.9	61.8	43.4	23.4	44.7	53.4	46.5M	41.7	63.6	45.8	38.2	60.4	41.0
ResNet101 [20]	56.7M	38.5	57.8	41.2	21.4	42.6	51.1	63.2M	40.4	61.1	44.2	36.4	57.7	38.8
ResNeXt101-32x4d [61]	56.4M	39.9	59.6	42.7	22.3	44.2	52.5	62.8M	41.9	62.5	45.9	37.5	59.4	40.2
PVT-Medium [56]	53.9M	41.9	63.1	44.3	25.0	44.9	57.6	63.9M	42.0	64.4	45.6	39.0	61.6	42.1
CycleMLP-B3	48.1M	42.5	63.2	45.3	25.2	45.5	56.2	58.0M	43.4	65.0	47.7	39.5	62.0	42.4
PVT-Large [56]	71.1M	42.6	63.7	45.4	25.8	46.0	58.4	81.0M	42.9	65.0	46.6	39.5	61.9	42.5
CycleMLP-B4	61.5M	43.2	63.9	46.2	26.6	46.5	57.4	71.5M	44.1	65.7	48.1	40.2	62.7	43.5
ResNeXt101-64x4d [61]	95.5M	41.0	60.9	44.0	23.9	45.2	54.0	101.9M	42.8	63.8	47.3	38.4	60.6	41.3
CycleMLP-B5	85.9M	42.7	63.3	45.3	24.1	46.3	57.4	95.3M	44.1	65.5	48.4	40.1	62.8	43.0

Table 5: **Object detection and instance segmentation on COCO val2017 [34].**

are initialized with ImageNet pre-trained weights and other newly added layers are initialized via Xavier [17]. We use the AdamW [37] optimizer with the initial learning rate of 1×10^{-4} . All models are trained on 8 Tesla V100 GPUs with a total batch size of 16 for 12 epochs (*i.e.*, $1 \times$ training scheduler). The input images are resized to the shorted side of 800 pixels and the longer side does not exceed 1333 pixels during training. We do not use the multi-scale [5, 70, 45] training strategy. In the testing stage, the shorter side of input images is resized to 800 pixels while no constraint on the longer side.

Results. As shown in Table 5, CycleMLP-based RetinaNet consistently surpasses the CNN-based ResNet [20], ResNeXt [61] and Transformer-based PVT [56] under similar parameter constraints, indicating that CycleMLP can serve as an excellent general-purpose backbone. Furthermore, using Mask R-CNN [19] for instance segmentation also demonstrates similar comparison results. For example, with RetinaNet, CycleMLP-B4 outperforms PVT-Large [56] by 0.6 AP while using less parameters (61.5M *v.s.* 71.1M).

4.4. Semantic Segmentation

Settings. We conduct semantic segmentation experiments on ADE20K [69] dataset, which covers a broad range of 150 semantic categories. ADE20K contains 20K training, 2K validation and 3K testing images. We adopt the `mmsegmentation` [7] toolbox as our codebase in this subsection. The experimental settings mostly follow PVT [56], which trains models for 40K iterations on 8 Tesla V100 GPUs with 4 samples per GPU. The backbone is initialized with the pre-trained weights on ImageNet. All models are optimized by AdamW [37]. The initial learning rate is configured as 2×10^{-4} with the polynomial decay parameter of 0.9. Input images are randomly resized and cropped to 512×512 at the training phase. During testing, we scale

Backbone	Semantic FPN	
	Param	mIoU (%)
ResNet18 [20]	15.5M	32.9
PVT-Tiny [56]	17.0M	35.7
CycleMLP-B1 (ours)	18.9M	39.5
ResNet50 [20]	28.5M	36.7
PVT-Small [56]	28.2M	39.8
Swin-T [†] [36]	31.9M	41.5
GFNet-Tiny [41]	26.6M	41.0
CycleMLP-B2 (ours)	30.6M	42.4
ResNet101 [20]	47.5M	38.8
ResNeXt101-32x4d [61]	47.1M	39.7
PVT-Medium [56]	48.0M	41.6
GFNet-Small [41]	47.5M	42.5
CycleMLP-B3 (ours)	42.1M	44.5
PVT-Large [56]	65.1M	42.1
Swin-S [†] [36]	53.2M	45.2
CycleMLP-B4 (ours)	55.6M	45.1
GFNet-Base [41]	74.7M	44.8
ResNeXt101-64x4d [61]	86.4M	40.2
CycleMLP-B5 (ours)	79.4M	45.6

Table 6: **Semantic segmentation on ADE20K [69] val.** All models are equipped with Semantic FPN [28]. [†] Results are from GFNet [41].

the images to the shorted side of 512. We adopt the simple approach Semantic FPN [28] as the semantic segmentation method following [56] for fair comparison.

Results. The results are shown in Table 6. CycleMLP outperforms ResNet [20] and PVT [56] significantly with similar parameters. Moreover, compared to the state-of-the-art Transformer-based backbone, Swin Transformer [36], CycleMLP can obtain comparable or even better performance. Specifically, CycleMLP-B2 surpasses Swin-T by 0.9 mIoU

with slightly less parameters (30.6M v.s. 31.9M).

Though GFNet [41] achieves similar performance as CycleMLP on ImageNet classification, CycleMLP notably outperforms GFNet on ADE20K semantic segmentation where input scale varies. We attribute the superiority of CycleMLP under a scale-variable scenario to the capability of dealing with arbitrary scales. On the contrary, GFNet [41] requires additional heuristic operation (weight interpolation) when the input scale varies, which may hurt the performance.

5. Conclusion

We present a versatile MLP-like architecture, CycleMLP, in this work. CycleMLP is built upon the Cycle Fully-Connected Layer (Cycle FC), which is capable to deal with variable input scales and can serve as a generic, plug-and-play replacement of vanilla FC layers. Experimental results demonstrate that CycleMLP outperforms existing MLP-like models on ImageNet classification and achieves promising performance on dense prediction tasks, *i.e.*, object detection, instance segmentation and semantic segmentation. This work shows that a transformer-free architecture can also serve as a general vision backbone.

References

- [1] Anurag Arnab, Mostafa Dehghani, Georg Heigold, Chen Sun, Mario Lučić, and Cordelia Schmid. Vivit: A video vision transformer. *arXiv preprint arXiv:2103.15691*, 2021. 3
- [2] Jimmy Lei Ba, Jamie Ryan Kiros, and Geoffrey E Hinton. Layer normalization. *arXiv preprint arXiv:1607.06450*, 2016. 3, 4
- [3] Gedas Bertasius, Heng Wang, and Lorenzo Torresani. Is space-time attention all you need for video understanding? *arXiv preprint arXiv:2102.05095*, 2021. 3
- [4] Tom B Brown, Benjamin Mann, Nick Ryder, Melanie Subbiah, Jared Kaplan, Prafulla Dhariwal, Arvind Neelakantan, Pranav Shyam, Girish Sastry, Amanda Askell, et al. Language models are few-shot learners. *arXiv preprint arXiv:2005.14165*, 2020. 3
- [5] Nicolas Carion, Francisco Massa, Gabriel Synnaeve, Nicolas Usunier, Alexander Kirillov, and Sergey Zagoruyko. End-to-end object detection with transformers. In *European Conference on Computer Vision*, pages 213–229. Springer, 2020. 2, 8
- [6] Kai Chen, Jiaqi Wang, Jiangmiao Pang, Yuhang Cao, Yu Xiong, Xiaoxiao Li, Shuyang Sun, Wansen Feng, Ziwei Liu, Jiarui Xu, Zheng Zhang, Dazhi Cheng, Chenchen Zhu, Tianheng Cheng, Qijie Zhao, Buyu Li, Xin Lu, Rui Zhu, Yue Wu, Jifeng Dai, Jingdong Wang, Jianping Shi, Wanli Ouyang, Chen Change Loy, and Dahua Lin. MMDetection: Open mmlab detection toolbox and benchmark. *arXiv preprint arXiv:1906.07155*, 2019. 7
- [7] MMSegmentation Contributors. MMSegmentation: Openmmlab semantic segmentation toolbox and benchmark. <https://github.com/open-mmlab/mmdetection>, 2020. 8
- [8] James W Cooley and John W Tukey. An algorithm for the machine calculation of complex fourier series. *Mathematics of computation*, 19(90):297–301, 1965. 6
- [9] Marius Cordts, Mohamed Omran, Sebastian Ramos, Timo Rehfeld, Markus Enzweiler, Rodrigo Benenson, Uwe Franke, Stefan Roth, and Bernt Schiele. The cityscapes dataset for semantic urban scene understanding. In *Proceedings of the IEEE conference on computer vision and pattern recognition*, pages 3213–3223, 2016. 2
- [10] Ekin D Cubuk, Barret Zoph, Jonathon Shlens, and Quoc V Le. Randaugment: Practical automated data augmentation with a reduced search space. In *Proceedings of the IEEE/CVF Conference on Computer Vision and Pattern Recognition Workshops*, pages 702–703, 2020. 3, 6
- [11] Jia Deng, Wei Dong, Richard Socher, Li-Jia Li, Kai Li, and Li Fei-Fei. Imagenet: A large-scale hierarchical image database. In *2009 IEEE conference on computer vision and pattern recognition*, pages 248–255. Ieee, 2009. 2, 3, 5, 6
- [12] Jacob Devlin, Ming-Wei Chang, Kenton Lee, and Kristina Toutanova. Bert: Pre-training of deep bidirectional transformers for language understanding. *arXiv preprint arXiv:1810.04805*, 2018. 3
- [13] Alexey Dosovitskiy, Lucas Beyer, Alexander Kolesnikov, Dirk Weissenborn, Xiaohua Zhai, Thomas Unterthiner, Mostafa Dehghani, Matthias Minderer, Georg Heigold, Sylvain Gelly, et al. An image is worth 16x16 words: Transformers for image recognition at scale. *arXiv preprint arXiv:2010.11929*, 2020. 1, 2, 3, 4, 7
- [14] Maksim Dzabraev, Maksim Kalashnikov, Stepan Komkov, and Aleksandr Petiushko. Mdmmt: Multidomain multimodal transformer for video retrieval. In *Proceedings of the IEEE/CVF Conference on Computer Vision and Pattern Recognition*, pages 3354–3363, 2021. 3
- [15] Haoqi Fan, Bo Xiong, Karttikeya Mangalam, Yanghao Li, Zhicheng Yan, Jitendra Malik, and Christoph Feichtenhofer. Multiscale vision transformers. *arXiv preprint arXiv:2104.11227*, 2021. 3, 4
- [16] Valentin Gabeur, Chen Sun, Karteek Alahari, and Cordelia Schmid. Multi-modal transformer for video retrieval. In *Computer Vision—ECCV 2020: 16th European Conference, Glasgow, UK, August 23–28, 2020, Proceedings, Part IV 16*, pages 214–229. Springer, 2020. 3
- [17] Xavier Glorot and Yoshua Bengio. Understanding the difficulty of training deep feedforward neural networks. In *Proceedings of the thirteenth international conference on artificial intelligence and statistics*, pages 249–256. JMLR Workshop and Conference Proceedings, 2010. 8
- [18] Meng-Hao Guo, Zheng-Ning Liu, Tai-Jiang Mu, and Shi-Min Hu. Beyond self-attention: External attention using two linear layers for visual tasks. *arXiv preprint arXiv:2105.02358*, 2021. 6
- [19] Kaiming He, Georgia Gkioxari, Piotr Dollár, and Ross Girshick. Mask r-cnn. In *Proceedings of the IEEE international conference on computer vision*, pages 2961–2969, 2017. 7, 8

- [20] Kaiming He, Xiangyu Zhang, Shaoqing Ren, and Jian Sun. Deep residual learning for image recognition. In *Proceedings of the IEEE conference on computer vision and pattern recognition*, pages 770–778, 2016. 1, 2, 3, 4, 5, 7, 8
- [21] Dan Hendrycks and Kevin Gimpel. Gaussian error linear units (gelus). *arXiv preprint arXiv:1606.08415*, 2016. 4
- [22] Qibin Hou, Zihang Jiang, Li Yuan, Ming-Ming Cheng, Shuicheng Yan, and Jiashi Feng. Vision permutator: A permutable mlp-like architecture for visual recognition. *arXiv preprint arXiv:2106.12368*, 2021. 3, 6
- [23] Andrew G Howard, Menglong Zhu, Bo Chen, Dmitry Kalenichenko, Weijun Wang, Tobias Weyand, Marco Andreetto, and Hartwig Adam. Mobilenets: Efficient convolutional neural networks for mobile vision applications. *arXiv preprint arXiv:1704.04861*, 2017. 2
- [24] Gao Huang, Zhuang Liu, Laurens van der Maaten, and Kilian Q Weinberger. Densely connected convolutional networks. In *Proceedings of the IEEE Conference on Computer Vision and Pattern Recognition*, 2017. 3
- [25] Gao Huang, Yu Sun, Zhuang Liu, Daniel Sedra, and Kilian Q Weinberger. Deep networks with stochastic depth. In *European conference on computer vision*, pages 646–661. Springer, 2016. 6
- [26] Zilong Huang, Xinggang Wang, Lichao Huang, Chang Huang, Yunchao Wei, and Wenyu Liu. Ccnet: Criss-cross attention for semantic segmentation. In *Proceedings of the IEEE/CVF International Conference on Computer Vision*, pages 603–612, 2019. 5
- [27] Sergey Ioffe and Christian Szegedy. Batch normalization: Accelerating deep network training by reducing internal covariate shift. In *International conference on machine learning*, pages 448–456. PMLR, 2015. 3
- [28] Alexander Kirillov, Ross Girshick, Kaiming He, and Piotr Dollár. Panoptic feature pyramid networks. In *Proceedings of the IEEE/CVF Conference on Computer Vision and Pattern Recognition*, pages 6399–6408, 2019. 8
- [29] Alex Krizhevsky, Ilya Sutskever, and Geoffrey E Hinton. Imagenet classification with deep convolutional neural networks. *Advances in neural information processing systems*, 25:1097–1105, 2012. 1, 3
- [30] Yann LeCun, Bernhard Boser, John S Denker, Donnie Henderson, Richard E Howard, Wayne Hubbard, and Lawrence D Jackel. Backpropagation applied to handwritten zip code recognition. *Neural computation*, 1(4):541–551, 1989. 3
- [31] Changlin Li, Tao Tang, Guangrun Wang, Jiefeng Peng, Bing Wang, Xiaodan Liang, and Xiaojun Chang. Bossnas: Exploring hybrid cnn-transformers with block-wisely self-supervised neural architecture search. *arXiv preprint arXiv:2103.12424*, 2021. 3
- [32] Min Lin, Qiang Chen, and Shuicheng Yan. Network in network. *arXiv preprint arXiv:1312.4400*, 2013. 2
- [33] Tsung-Yi Lin, Priya Goyal, Ross Girshick, Kaiming He, and Piotr Dollár. Focal loss for dense object detection. In *Proceedings of the IEEE international conference on computer vision*, pages 2980–2988, 2017. 7
- [34] Tsung-Yi Lin, Michael Maire, Serge Belongie, James Hays, Pietro Perona, Deva Ramanan, Piotr Dollár, and C Lawrence Zitnick. Microsoft coco: Common objects in context. In *European conference on computer vision*, pages 740–755. Springer, 2014. 2, 3, 5, 7, 8
- [35] Hanxiao Liu, Zihang Dai, David R So, and Quoc V Le. Pay attention to mlps. *arXiv preprint arXiv:2105.08050*, 2021. 1, 3, 6
- [36] Ze Liu, Yutong Lin, Yue Cao, Han Hu, Yixuan Wei, Zheng Zhang, Stephen Lin, and Baining Guo. Swin transformer: Hierarchical vision transformer using shifted windows. *arXiv preprint arXiv:2103.14030*, 2021. 1, 2, 3, 4, 6, 7, 8
- [37] Ilya Loshchilov and Frank Hutter. Decoupled weight decay regularization. *arXiv preprint arXiv:1711.05101*, 2017. 6, 8
- [38] Adam Paszke, Sam Gross, Francisco Massa, Adam Lerer, James Bradbury, Gregory Chanan, Trevor Killeen, Zeming Lin, Natalia Gimelshein, Luca Antiga, Alban Desmaison, Andreas Kopf, Edward Yang, Zachary DeVito, Martin Raison, Alykhan Tejani, Sasank Chilamkurthy, Benoit Steiner, Lu Fang, Junjie Bai, and Soumith Chintala. Pytorch: An imperative style, high-performance deep learning library. In H. Wallach, H. Larochelle, A. Beygelzimer, F. d’Alché-Buc, E. Fox, and R. Garnett, editors, *Advances in Neural Information Processing Systems 32*, pages 8024–8035. Curran Associates, Inc., 2019. 6
- [39] Alec Radford, Jong Wook Kim, Chris Hallacy, Aditya Ramesh, Gabriel Goh, Sandhini Agarwal, Girish Sastry, Amanda Askell, Pamela Mishkin, Jack Clark, et al. Learning transferable visual models from natural language supervision. *arXiv preprint arXiv:2103.00020*, 2021. 3
- [40] Ilija Radosavovic, Raj Prateek Kosaraju, Ross Girshick, Kaiming He, and Piotr Dollár. Designing network design spaces. In *Proceedings of the IEEE/CVF Conference on Computer Vision and Pattern Recognition*, pages 10428–10436, 2020. 7
- [41] Yongming Rao, Wenliang Zhao, Zheng Zhu, Jiwen Lu, and Jie Zhou. Global filter networks for image classification. *arXiv preprint arXiv:2107.00645*, 2021. 6, 7, 8, 9
- [42] David E Rumelhart, Geoffrey E Hinton, and Ronald J Williams. Learning representations by back-propagating errors. *nature*, 323(6088):533–536, 1986. 5
- [43] Karen Simonyan and Andrew Zisserman. Very deep convolutional networks for large-scale image recognition. *arXiv preprint arXiv:1409.1556*, 2014. 1, 2, 3, 4
- [44] Aravind Srinivas, Tsung-Yi Lin, Niki Parmar, Jonathon Shlens, Pieter Abbeel, and Ashish Vaswani. Bottleneck transformers for visual recognition. In *Proceedings of the IEEE/CVF Conference on Computer Vision and Pattern Recognition*, pages 16519–16529, 2021. 3, 7
- [45] Peize Sun, Rufeng Zhang, Yi Jiang, Tao Kong, Chenfeng Xu, Wei Zhan, Masayoshi Tomizuka, Lei Li, Zehuan Yuan, Changhu Wang, et al. Sparse r-cnn: End-to-end object detection with learnable proposals. In *Proceedings of the IEEE/CVF Conference on Computer Vision and Pattern Recognition*, pages 14454–14463, 2021. 8
- [46] Christian Szegedy, Wei Liu, Yangqing Jia, Pierre Sermanet, Scott Reed, Dragomir Anguelov, Dumitru Erhan, Vincent Vanhoucke, and Andrew Rabinovich. Going deeper with

- convolutions. In *Proceedings of the IEEE conference on computer vision and pattern recognition*, pages 1–9, 2015. [2](#)
- [47] Christian Szegedy, Vincent Vanhoucke, Sergey Ioffe, Jon Shlens, and Zbigniew Wojna. Rethinking the inception architecture for computer vision. In *Proceedings of the IEEE conference on computer vision and pattern recognition*, pages 2818–2826, 2016. [5](#)
- [48] Mingxing Tan and Quoc Le. Efficientnet: Rethinking model scaling for convolutional neural networks. In *International Conference on Machine Learning*, pages 6105–6114. PMLR, 2019. [7](#)
- [49] Ilya Tolstikhin, Neil Houlsby, Alexander Kolesnikov, Lucas Beyer, Xiaohua Zhai, Thomas Unterthiner, Jessica Yung, Daniel Keysers, Jakob Uszkoreit, Mario Lucic, et al. Mlp-mixer: An all-mlp architecture for vision. *arXiv preprint arXiv:2105.01601*, 2021. [1](#), [2](#), [3](#), [4](#), [6](#)
- [50] Hugo Touvron, Piotr Bojanowski, Mathilde Caron, Matthieu Cord, Alaaeldin El-Nouby, Edouard Grave, Armand Joulin, Gabriel Synnaeve, Jakob Verbeek, and Hervé Jégou. Resmlp: Feedforward networks for image classification with data-efficient training. *arXiv preprint arXiv:2105.03404*, 2021. [1](#), [3](#), [6](#)
- [51] Hugo Touvron, Matthieu Cord, Matthijs Douze, Francisco Massa, Alexandre Sablayrolles, and Hervé Jégou. Training data-efficient image transformers & distillation through attention. *arXiv preprint arXiv:2012.12877*, 2020. [1](#), [3](#), [6](#), [7](#)
- [52] Hugo Touvron, Matthieu Cord, Alexandre Sablayrolles, Gabriel Synnaeve, and Hervé Jégou. Going deeper with image transformers. *arXiv preprint arXiv:2103.17239*, 2021. [3](#)
- [53] Ashish Vaswani, Noam Shazeer, Niki Parmar, Jakob Uszkoreit, Llion Jones, Aidan N Gomez, Łukasz Kaiser, and Illia Polosukhin. Attention is all you need. In *Advances in neural information processing systems*, pages 5998–6008, 2017. [1](#)
- [54] Alex Wang, Amanpreet Singh, Julian Michael, Felix Hill, Omer Levy, and Samuel R Bowman. Glue: A multi-task benchmark and analysis platform for natural language understanding. *arXiv preprint arXiv:1804.07461*, 2018. [3](#)
- [55] Wenhai Wang, Enze Xie, Xiang Li, Deng-Ping Fan, Kaitao Song, Ding Liang, Tong Lu, Ping Luo, and Ling Shao. Pvtv2: Improved baselines with pyramid vision transformer. *arXiv preprint arXiv:2106.13797*, 2021. [4](#)
- [56] Wenhai Wang, Enze Xie, Xiang Li, Deng-Ping Fan, Kaitao Song, Ding Liang, Tong Lu, Ping Luo, and Ling Shao. Pyramid vision transformer: A versatile backbone for dense prediction without convolutions. *arXiv preprint arXiv:2102.12122*, 2021. [3](#), [4](#), [7](#), [8](#)
- [57] Yuqing Wang, Zhaoliang Xu, Xinlong Wang, Chunhua Shen, Baoshan Cheng, Hao Shen, and Huaxia Xia. End-to-end video instance segmentation with transformers. In *Proceedings of the IEEE/CVF Conference on Computer Vision and Pattern Recognition*, pages 8741–8750, 2021. [3](#)
- [58] Ross Wightman. Pytorch image models. <https://github.com/rwightman/pytorch-image-models>, 2019. [6](#)
- [59] Haiping Wu, Bin Xiao, Noel Codella, Mengchen Liu, Xiyang Dai, Lu Yuan, and Lei Zhang. Cvt: Introducing convolutions to vision transformers. *arXiv preprint arXiv:2103.15808*, 2021. [3](#)
- [60] Enze Xie, Wenhai Wang, Zhiding Yu, Anima Anandkumar, Jose M Alvarez, and Ping Luo. Segformer: Simple and efficient design for semantic segmentation with transformers. *arXiv preprint arXiv:2105.15203*, 2021. [3](#)
- [61] Saining Xie, Ross Girshick, Piotr Dollár, Zhuowen Tu, and Kaiming He. Aggregated residual transformations for deep neural networks. In *Proceedings of the IEEE conference on computer vision and pattern recognition*, pages 1492–1500, 2017. [8](#)
- [62] Zhilin Yang, Zihang Dai, Yiming Yang, Jaime Carbonell, Russ R Salakhutdinov, and Quoc V Le. Xlnet: Generalized autoregressive pretraining for language understanding. *Advances in neural information processing systems*, 32, 2019. [3](#)
- [63] Tan Yu, Xu Li, Yunfeng Cai, Mingming Sun, and Ping Li. S²-mlp: Spatial-shift mlp architecture for vision. *arXiv preprint arXiv:2106.07477*, 2021. [3](#), [6](#)
- [64] Li Yuan, Yunpeng Chen, Tao Wang, Weihao Yu, Yujun Shi, Zihang Jiang, Francis EH Tay, Jiashi Feng, and Shuicheng Yan. Tokens-to-token vit: Training vision transformers from scratch on imagenet. *arXiv preprint arXiv:2101.11986*, 2021. [3](#)
- [65] Sangdoon Yun, Dongyoon Han, Seong Joon Oh, Sanghyuk Chun, Junsuk Choe, and Youngjoon Yoo. Cutmix: Regularization strategy to train strong classifiers with localizable features. In *Proceedings of the IEEE/CVF International Conference on Computer Vision*, pages 6023–6032, 2019. [3](#), [6](#)
- [66] Hongyi Zhang, Moustapha Cisse, Yann N Dauphin, and David Lopez-Paz. mixup: Beyond empirical risk minimization. *arXiv preprint arXiv:1710.09412*, 2017. [3](#), [6](#)
- [67] Sixiao Zheng, Jiachen Lu, Hengshuang Zhao, Xiatian Zhu, Zekun Luo, Yabiao Wang, Yanwei Fu, Jianfeng Feng, Tao Xiang, Philip HS Torr, et al. Rethinking semantic segmentation from a sequence-to-sequence perspective with transformers. In *Proceedings of the IEEE/CVF Conference on Computer Vision and Pattern Recognition*, pages 6881–6890, 2021. [3](#)
- [68] Zhun Zhong, Liang Zheng, Guoliang Kang, Shaozi Li, and Yi Yang. Random erasing data augmentation. In *Proceedings of the AAAI Conference on Artificial Intelligence*, volume 34, pages 13001–13008, 2020. [6](#)
- [69] Bolei Zhou, Hang Zhao, Xavier Puig, Sanja Fidler, Adela Barriuso, and Antonio Torralba. Scene parsing through ade20k dataset. In *Proceedings of the IEEE conference on computer vision and pattern recognition*, pages 633–641, 2017. [2](#), [3](#), [5](#), [8](#)
- [70] Xizhou Zhu, Weijie Su, Lewei Lu, Bin Li, Xiaogang Wang, and Jifeng Dai. Deformable detr: Deformable transformers for end-to-end object detection. *arXiv preprint arXiv:2010.04159*, 2020. [8](#)